environments

MDPI

Article

Ti/IrO_2–RuO_2 Electrode for Electrochemical Oxidation of Reverse Osmosis Pesticide Concentrate Wastewater: Performance Evaluation, Parameter Optimization and Degradation Mechanism

Yang Pu [1], Yu Cao [1], Mingxin Zhu [1,*], Hua Zhou [1], Zhiying Liu [1], Zhu He [2] and Jianzhong Jiang [2]

[1] School of Environmental Science and Engineering, Nanjing Tech University, Nanjing 211816, China; 15366331880@163.com (Y.P.); 202361202043@njtech.edu.cn (Y.C.); zhouhua@njtech.edu.cn (H.Z.); zhiying555@njtech.edu.cn (Z.L.)

[2] Defense Engineering Institute, Academy of Military Sciences, People's Liberation Army of China, Beijing 100036, China; hezhu1029@163.com (Z.H.); jmmhh@sina.com (J.J.)

* Correspondence: zmx@njtech.edu.cn

Abstract

Electrocatalytic oxidation technology demonstrates significant potential in treating refractory industrial wastewater, playing a crucial role in industrial pollution control. This paper established an electrocatalytic oxidation system using Ti/IrO_2–RuO_2 as the anode for pretreating high-salinity, refractory pesticide and chemical membrane concentrate. The optimal conditions were identified through a systematic investigation of key parameters including salt concentration, current density, initial pH, and electrode spacing as follows: salt concentration of 15 g/L, current density of 43.69 mA/cm^2, initial pH of 5.0, and electrode spacing of 2.0 cm, achieving a maximum COD removal rate of 93.45% with energy consumption of 0.191 (kW h)/kg COD. The results indicated that this system effective degraded organic compounds in membrane concentrate. These findings provided innovative approaches for the efficient treatment of refractory organic wastewater from pesticide and chemical industries.

Keywords: electrocatalytic oxidation; Ti/IrO_2–RuO_2; membrane concentrate

Check for updates

Academic Editor: Alfredo Cassano

Received: 28 March 2026
Revised: 11 May 2026
Accepted: 20 May 2026
Published: 25 May 2026

Copyright: © 2026 by the authors. Licensee MDPI, Basel, Switzerland. This article is an open access article distributed under the terms and conditions of the Creative Commons Attribution (CC BY) license.

1. Introduction

In modern agricultural production, pesticides play a crucial role in increasing crop yields, controlling pests and plant diseases. Pesticides can be classified into insecticides, acaricides, fungicides, herbicides, and plant growth regulators based on their functional characteristics [1]. Currently, the global pesticide usage is 3.73 million tons with China's annual pesticide production exceeding 1 million tons and usage reaching 783,200 tons [2]. However, due to the complex synthetic procedures, high equipment requirements, and low raw material utilization rates in pesticide production, synthetic intermediates often exist in wastewater as high-concentration pollutants. Product purification and equipment cleaning also generate substantial intermediate wastewater [3,4]. These intermediates are mostly long-chain and heterocyclic macromolecular organic compounds [5]. Pesticide chemical wastewater is characterized by high COD, high toxicity, complex composition, and difficulty in degradation.

For refractory wastewater from pesticide and chemical industries, the current standard approach involves a "pretreatment–biological treatment–deep treatment" integrated

process [6]. During deep treatment, membrane-based methods such as reverse osmosis (RO) are predominantly employed. This process generates 25–45% of the treated water as membrane concentrate [7,8]. Due to its high pollutant concentration and salt content (COD ranging 500–2500, salt content ranging 20,000–30,000 mg/L), biochemical treatment proves challenging, necessitating physicochemical methods for disposal. Evaporation technology enables both a volume reduction and resource recovery of membrane concentrate. Among these, mechanical vapor recovery (MVR) stands out as an energy-efficient solution widely adopted in evaporation crystallization systems [9]. However, direct discharge of membrane concentrate into MVR evaporators may cause scaling, impure salt crystallization, and substandard condensate quality due to its high organic content, ammonia nitrogen, and hardness ions, thus requiring pretreatment [10]. Current pretreatment processes, however, face challenges like high costs and inconsistent performance. While advanced oxidation methods like ozone are commonly used for organic wastewater treatment, they remain expensive and ineffective against high-concentration pollutants. Thus, developing efficient treatment methods for organic contaminants in concentrated wastewater remains pivotal to achieving zero liquid discharge (ZLD) in pesticide and chemical industries.

Electrocatalytic oxidation, as an advanced oxidation technology, can efficiently treat various high-concentration organic wastewater, particularly pesticide and chemical wastewater with a high content of refractory organic compounds [4]. The electrocatalytic oxidation reaction primarily degrades organic pollutants through direct oxidation at the anode or by generating highly oxidative hydroxyl radicals via the electrode [11,12].·OH radicals can break down organic molecules into smaller, less toxic or non-toxic molecules, or they can even directly mineralize them into CO_2 and H_2O, thereby improving the biodegradability of wastewater and facilitating subsequent biochemical treatment [13,14]. This technology is widely recognized in the industry for its advantages of simple reaction equipment, low cost, and high efficiency. Ke et al. employed a titanium substrate as the anode, SnO_2 + Sb_2O_3 as the intermediate layer, and β-PbO_2 as the outer layer (Ti/SnO_2 + Sb_2O_3/β-PbO_2) to systematically investigate the effects of titanium-loaded composite metals on the electrocatalytic oxidation of fertilizer wastewater with high salt–nitrogen and high ammonia–nitrogen content [15]. The results demonstrated the excellent COD removal efficiency of this system, achieving a 66.7% removal rate from an influent COD concentration of 12,000 mg/L to an effluent COD concentration of 4000 mg/L. When the Cl^- concentration was increased to 5%, the anode composed of titanium-supported SnO_2 + Sb_2O_3 as the interlayer and β-PbO_2 as the outer layer (Ti/SnO_2 + Sb_2O_3/β-PbO_2) was applied to the electrocatalytic treatment of actual wastewater, involving pharmaceutical intermediates and pesticides. This research demonstrated that the anode exhibited excellent catalytic oxidation performance particularly under high COD (12,000 mg/L) and high salinity conditions. Yang. [14] utilized a porous TiO_2-based electrocatalytic membrane reactor/carbon membrane anode for treating oily industrial wastewater, achieving removal rates of 86.2% for oil and 94.4% for COD, which were significantly higher than those of 78.6% and 83.7% observed with membrane filtration alone. These investigation implied that electrocatalysis holds broad application prospects in the field of refractory organic wastewater treatment.

However, due to the limitations of electrode materials and the complexity of industrial wastewater, there has been limited research on the electrocatalytic oxidation and degradation of pesticide wastewater [14]. Herein, this paper established an electrocatalytic experimental platform to systematically investigate key parameters affecting the system's performance, including COD removal efficiency and energy consumption evaluation for pesticide membrane concentrate. Furthermore, we examined the impact of factors such as salt concentration, current density, initial pH value, and plate spacing on electrocatalytic treatment effectiveness. Based on these, the degradation mechanism of membrane concen-

trate in the electrocatalytic oxidation system was elucidated, providing new insights for the efficient treatment of pesticide chemical wastewater.

2. Materials and Methods

2.1. Materials and Equipment

The membrane concentrate was supplied by Shandong Sino-Agri United Biotechnology Co., Ltd. (Jinan, China) The parameters of membrane concentrate are listed in Table 1.

Table 1. The parameters of membrane concentrate.

COD (mg/L)	NH_4^+-N(mg/L)	TN (mg/ L)	Conductivity (μS/ cm)	pH
600	405	707	6500	7.5

A self-built electrocatalytic reaction system for a laboratory was used in this paper. As observed in Figure 1, the reactor consists of an external power supply, electrodes, and an electrocatalytic device. The external power supply (SMG-50A) was purchased from Sanma Rectifier Technology Co., Ltd. (SuZhou, China). The electrocatalytic reactor had dimensions of 60 mm × 80 mm × 200 mm. The anode was a titanium-based iridium–ruthenium electrode plate provided by Suzhou Shurta Industrial Co., Ltd. (SuZhou, China). The cathode was a stainless steel electrode plate, which also purchased from Suzhou Shurta Industrial Co., Ltd.



Figure 1. The image of electrocatalytic reaction system.

2.2. Electrocatalysis Experiment

In this experiment, the pH of wastewater was adjusted by 1 mol/L NaOH and 1 mol/L H_2SO_4 aqueous solutions, while the conductivity was regulated with 0.1 mol/L NaCl. A total of 500 mL of treated water samples was added to the reactor. During the 90 min electrocatalytic process, samples were collected at time points of 10, 20, 40, 60, and 90 min. The effects of different experimental parameters on electrocatalytic oxidation performance were investigated by measuring the COD (Hach DRB 200, Shanghai, China) of filtered water samples. The results represent the average of three repeated tests with an error margin of less than 5.0%.

2.3. Characterization and Analysis

The electrocatalytic performance was evaluated based on the COD removal rate and energy consumption. The COD removal rate and energy consumption were calculated by Equations (1) and (2).

$$\mathrm{CDO_{removalrate}}(\%) = \frac{\mathrm{COD_o - COD_t}}{\mathrm{COD_o}} \times 100\%, \quad (1)$$

$$\text{Energy Consumption}(\mathrm{kWh/kg\ COD}) = \frac{\mathrm{U \cdot I \cdot T}}{(\mathrm{COD_o - COD_t}) \times \mathrm{V}}, \quad (2)$$

Here, COD_0 denoted the COD value of the membrane concentrate prior to electrocatalytic reaction (mg/L), while COD_t represents its post-reaction COD value (mg/L). The parameters include U (reaction voltage, V), I (reaction current, A), T (reaction time, h), and V (wastewater volume, L) in the electrocatalytic system.

3. Results and Discussion

3.1. Surface Morphology and Characterization

3.1.1. SEM Characterization and EDS Analysis of the Electrode

As shown in Figure 2, the surface of the Ir/Ru/Ti anode exhibits a typical mud-crack morphology composed of irregular granular domains separated by interconnected cracks. This characteristic structure, commonly formed during the thermal decomposition of metal oxide coatings, can effectively increase the real surface area and provide abundant electroactive sites. Meanwhile, the crack network facilitates electrolyte penetration and mass transfer, which is beneficial for enhancing the electrocatalytic oxidation performance. In addition, the coating appears relatively compact and uniformly distributed on the Ti substrate without obvious large-scale peeling, indicating good coating integrity and adhesion.

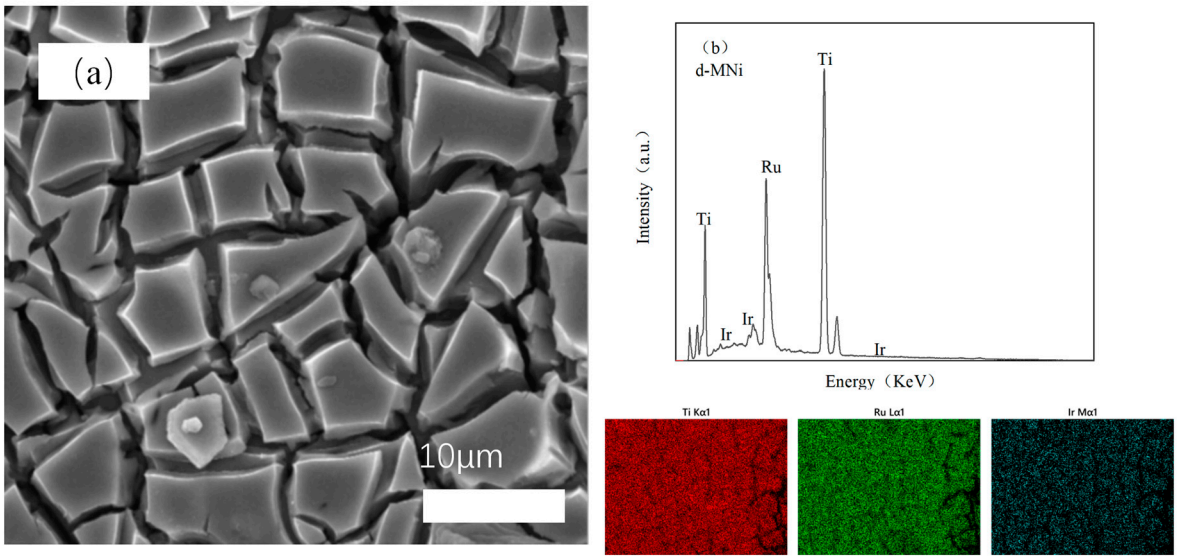

Figure 2. Morphological characterization of the IrO_2–RuO_2/Ti electrode: (**a**) SEM image and (**b**) EDS analysis.

The EDS spectrum confirms the presence of Ti, Ru, and Ir elements on the electrode surface, demonstrating that the active Ir/Ru oxide coating was successfully deposited on the Ti substrate. Elemental mapping further reveals that Ti, Ru, and Ir are distributed relatively uniformly across the surface with no obvious elemental segregation or localized agglomeration. Such a homogeneous distribution of active components is favorable for

ensuring stable electrocatalytic activity and improving the durability of the anode during electrochemical operation. Overall, the SEM and EDS results indicate that the prepared Ir/Ru/Ti electrode possesses a well-developed surface morphology and uniform elemental composition, which are advantageous for electrochemical oxidation applications.

3.1.2. XRD Results Analysis

Figure 3 presents the XRD pattern of the Ir–Ru–Ti electrode. The major diffraction peaks observed at 2θ values of approximately 35°, 38°, 40°, 53°, 63°, 70°, and 76° can be well indexed to the Ti substrate (PDF#44-1294), indicating that the substrate maintained good crystallinity after the coating and thermal treatment processes. The strong intensity of the Ti reflections also suggests that the active layer was relatively thin, allowing the diffraction signal from the underlying substrate to remain prominent. In addition, the reflections located near 2θ = 27° and 36° are attributable to TiO_2, implying that a surface oxide layer formed on the Ti substrate during thermal treatment. Such a TiO_2 interlayer is generally considered beneficial for improving the adhesion and stability of the coating. Several weak reflections were also consistent with the reference pattern of Ir (PDF#46-1044), confirming the incorporation of Ir-containing species into the electrode coating. However, no distinct diffraction peaks assignable exclusively to Ru or RuO_2 were identified. This may be due to the relatively low Ru content, limited crystallinity, or overlap of Ru-related peaks with those of Ti, TiO_2, and Ir-containing phases. Therefore, the XRD results suggest that the electrode surface was composed of a Ti substrate covered by a TiO_2 transition layer and Ir-containing active phases, while the Ru species were likely present in a poorly crystalline state or highly dispersed within the coating matrix. Such a structural feature is favorable for maintaining the integrity and electrocatalytic activity of the electrode during electrochemical oxidation.

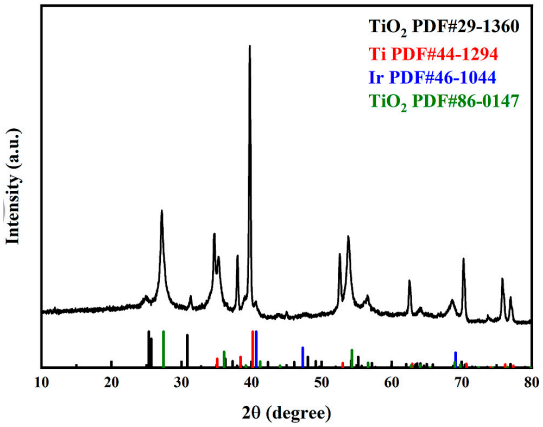

Figure 3. XRD pattern of the IrO_2–RuO_2/Ti electrode.

3.2. Electrochemical Characterization

3.2.1. LSV and CV Analyses of the Ir–Ru–Ti Electrode

Figure 4a,b presents the LSV and CV curves of the IrO_2–RuO_2/Ti anode in 0.5 mol L^{-1} NaCl. In the LSV profile, the anodic current increases sharply at 1.05–1.10 V, indicating the onset of a rapid anodic oxidation process, which is mainly attributed to the chlorine evolution reaction in chloride electrolyte. The low onset potential suggests high electrocatalytic activity of the electrode toward chloride oxidation. The CV response is in good agreement with the LSV result, showing a pronounced anodic current increase above ~1.10 V. Meanwhile, the broad current response in the low-potential region reflects the pseudocapacitive nature of the mixed Ir/Ru oxide coating, arising from surface redox transitions of the active species. A discernible cathodic feature is observed in the reverse

scan, indicating a partial reduction in the oxidized surface species and thus a certain degree of reversibility of the interfacial redox process. Overall, the IrO_2–RuO_2/Ti anode exhibits a low chlorine evolution onset potential, fast interfacial charge-transfer behavior, and good electrochemical stability, confirming its suitability as an efficient chlorine-evolving dimensionally stable anode in chloride-containing media.

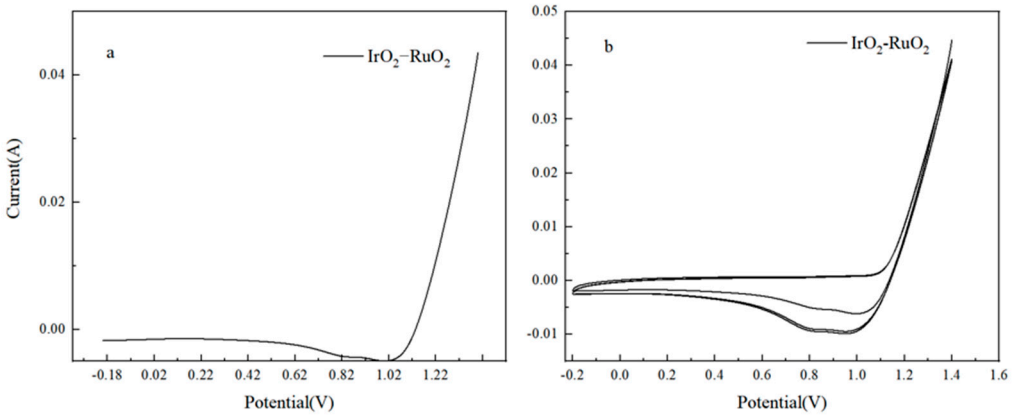

Figure 4. Electrochemical characterization of the IrO_2–RuO_2/Ti electrode: (**a**) linear sweep voltammetry (LSV) curve and (**b**) cyclic voltammetry (CV) curve.

3.2.2. Electrode SERVICE Life Test

As shown in Figure 5, the durability of the electrode was further evaluated by an accelerated lifetime test at 1000 mA/cm^2, and the accelerated lifetime was approximately 75 min. According to the equation $t_1 = (i_2/i_1)^2 t_2$, the estimated service lifetime of the electrode at the practical operating current density of 45 mA/cm^2 was 617.3 h. These results indicate that the IrO_2–RuO_2/Ti electrode exhibits high electrocatalytic activity and satisfactory durability, demonstrating its potential for practical electrochemical applications.

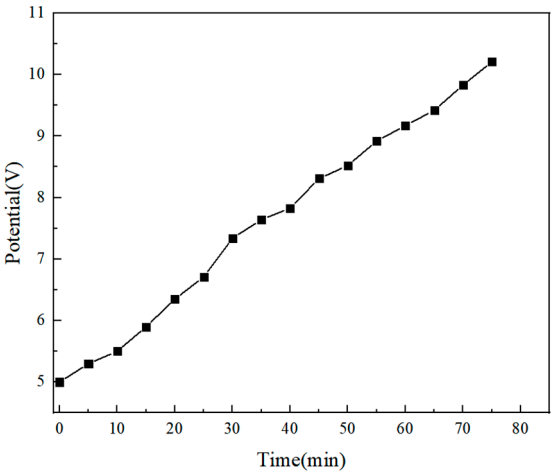

Figure 5. Accelerated lifetime test of the electrode.

3.3. Effect of Current Density on Electrocatalytic Oxidation Performance

Current density could significantly influence electrocatalysis by affecting the chloride evolution rate, playing a crucial role in catalytic performance [16]. The current density was changed from 35 to 65 mA/cm^2 to investigate its impact on membrane electrolysis efficiency, and the corresponding results are shown in Figure 6. The data indicated that the COD removal efficiency increased from 71.31% to 79.56% when the current density increased from 35 mA/cm^2 to 45 mA/cm^2 at the treat time of 90 min. However, further increases

in current density showed limited improvement. At 45 mA/cm^2, the COD removal rate reached 79.56% with an energy consumption of 0.245 (kW h)/kgCOD. When the current density increased to 65 mA/cm^2, the energy consumption rose by 0.15 (kW h)/kg COD, while the COD removal efficiency improved only 2%. This occurs because excessive current density promotes oxygen evolution reactions, reducing current efficiency [17]. Temperature analysis revealed that higher current densities caused temperature increases, converting electrical energy into heat and further degrading efficiency [18]. Elevated temperatures may also inactivate free radicals, hindering subsequent wastewater treatment processes. Based on a comparative analysis of COD removal efficiency and energy consumption across different current densities, the optimal current density in this experiment was determined to be 45 mA/cm^2.

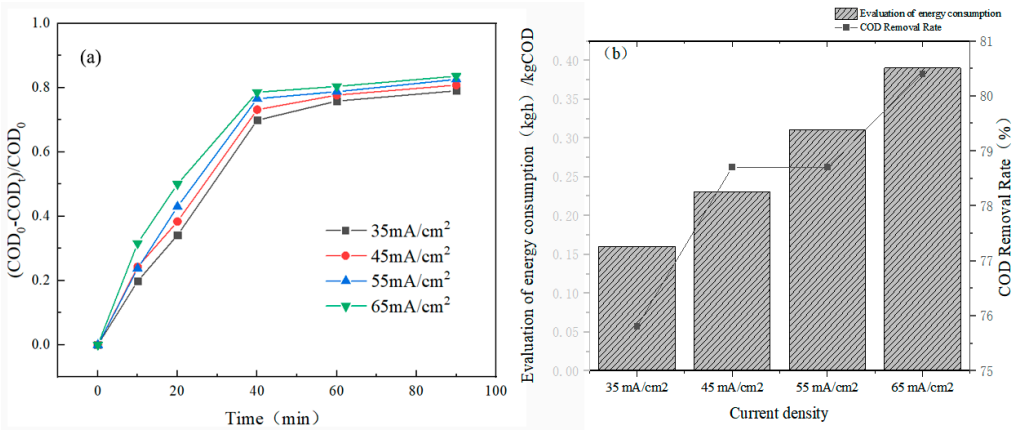

Figure 6. Effect of current density on electrocatalytic oxidation performance: (**a**) COD removal efficiency and (**b**) energy consumption.

3.4. Effect of Salt Concentration on Electrochemical Oxidation Performance

Variations in salt concentration significantly affect water conductivity, which critically influences electrode removal efficiency [19]. Figure 7a demonstrated COD removal rate changes under different NaCl addition conditions. Typically, conductivity in the reaction system increases markedly with rising salt concentration. When the salt concentration increased from 3 g/L to 13 g/L, the COD removal rate rose from 82.13% to 90.7%. At a salt concentration of 13 g/L, the COD removal rate reached 90.7% after 90 min of reaction time. However, the COD removal rate showed a gradual increase with further conductivity elevation. Compared to the 13 g/L salt concentration, the COD removal rate with salt concentration 18 g/L only increases by 0.78% after 90 min of treatment.

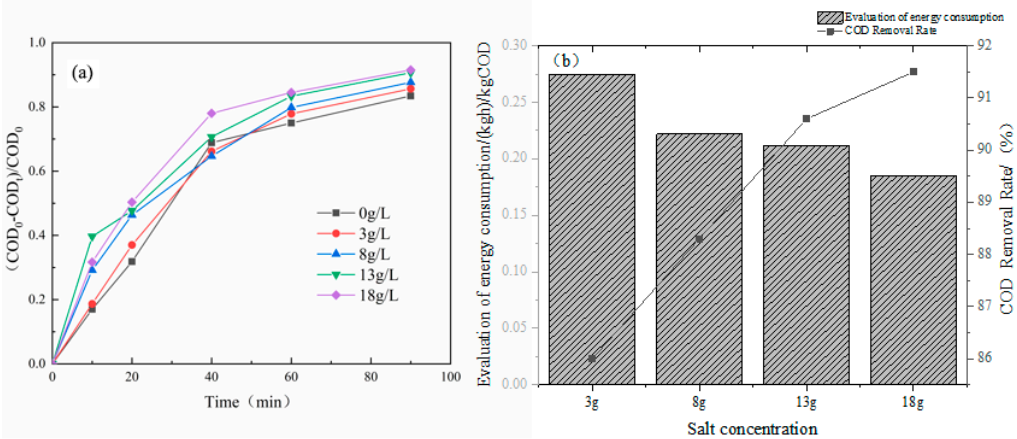

Figure 7. Effect of salt concentration on electrocatalytic oxidation performance: (**a**) COD removal efficiency and (**b**) energy consumption.

Figure 7b illustrates the relationship between system energy consumption and conductivity. The data demonstrated that the COD removal efficiency decreased with increasing conductivity. These findings confirmed that appropriate salt concentrations enhanced the conductivity of electrocatalytic reaction systems, accelerating both electron transfer and organic pollutant mass transfer rates in wastewater—a result consistent with previous studies [19]. When the salt concentration ranged from 3 g/L to 13 g/L, the COD degradation rate increased with the conductivity. This occurred because rising ionic concentrations intensify the non-uniform electric field between cathode/anode plates and electrodes under external power supply, accelerating organic pollutant reactions and effectively degrading macromolecular organic pollutants [20]. However, when the salt concentration increased from 13 g/L to 18 g/L, the 90-min COD removal rate rose by only 0.78%, indicating that the reaction was governed by organic oxidation kinetics rather than mass transfer. Further conductivity increases showed a negligible improvement in COD removal efficiency [21]. From energy-saving and cost-effective perspectives, 13 g/L was identified as the optimal conductivity for electrocatalytic oxidation systems.

3.5. Effect of pH Value on Electrochemical Oxidation Performance

pH value variations could significantly influence electrode treatment efficiency [21]. As shown in Figure 8, the initial pH value of the reaction system markedly affected electrochemical oxidation. At a pH of 5, the system achieved an 82.5% COD removal rate after 90 min with an energy consumption of 0.25 (kW h)/kg COD. During this process, hydroxyl radical reactions dominated as the primary mechanism for removing refractory organic compounds from wastewater [21]. Under anodic conditions, surface Cl^- ions released electrons to form Cl and Ru^{3+}, which were subsequently oxidized to Ru^{4+} via the circuit, accelerating chlorine evolution [22]. When the initial pH value dropped to 3, the COD removal rate decreased to 72% after 90 min of reaction time with a decrease of 10.5% compared with that at initial pH value of 5. And also, the energy consumption decreased to 1.1 (kW h)/kgCOD. This may be attributed to the acidic environment promoting H_2O_2 formation on the cathode surface, where H_2O_2 decomposed into ·OH upon temperature rise and generated adsorbed MO_x(·OH on the anode surface, thereby enhancing pollutant removal [23]. However, excessively low pH enhanced electrode corrosion and titanium substrate oxidation, thus reducing coating activity and electrochemical performance [24]. Under alkaline conditions, the removal efficiency was significantly reduced. At a pH value of 11, 2 h of electrochemical oxidation achieved only a 40.56% removal rate. This occurred because under alkaline conditions, the oxygen evolution potential of the electrode decreased, exacerbating the side reaction of oxygen evolution. Additionally, the active species ClO^- in the solution underwent reduction, leading to a decrease in the concentration of active chlorine in the solution, thereby reducing the oxidative capacity of the electrocatalytic oxidation system.

3.6. Impact of Plate Spacing on Electrocatalytic Oxidation Performance

The distance between electrodes significantly affected the diffusion rates of pollutants and dissolved oxygen in water, thereby substantially influencing the electrocatalytic oxidation performance. Figure 9a illustrates the COD removal rate and energy consumption of the system with different plate spacing. When the plate spacing was 3 cm, the COD removal rate reached 79.31%. When the plate spacing was adjusted to 2 cm, the COD removal rate increased to 92.87% within 90 min. These data indicated that reduced plate spacing significantly increased electrocatalytic oxidation performance. However, when the plate spacing further decrease to 1 cm, the COD removal rate decreased to 92.7%. This was primarily due to the limited plate spacing hindering the diffusion of organic pollutants in

the reaction system, leading to severe wastewater concentration polarization [24]. Such conditions also affected mass transfer rates in the solution, resulting in lower COD removal efficiency. Additionally, at smaller electrode distances, oxygen cannot adequately replenish the particle electrode surface, significantly reducing the generation efficiency of hydroxyl radicals and the degradation efficiency of organic pollutants [25]. The results demonstrated that increasing the spacing between polar plates within a certain range effectively reduced mass transfer resistance and enhanced hydroxyl radical generation rates, thereby improving organic pollutant removal efficiency and lowering processing costs [26]. However, excessive plate spacing increased the distance between convection and diffusion pathways, resulting in diminished mass concentration gradients and electrochemical reaction efficiency, ultimately degrading catalytic oxidation performance [27].

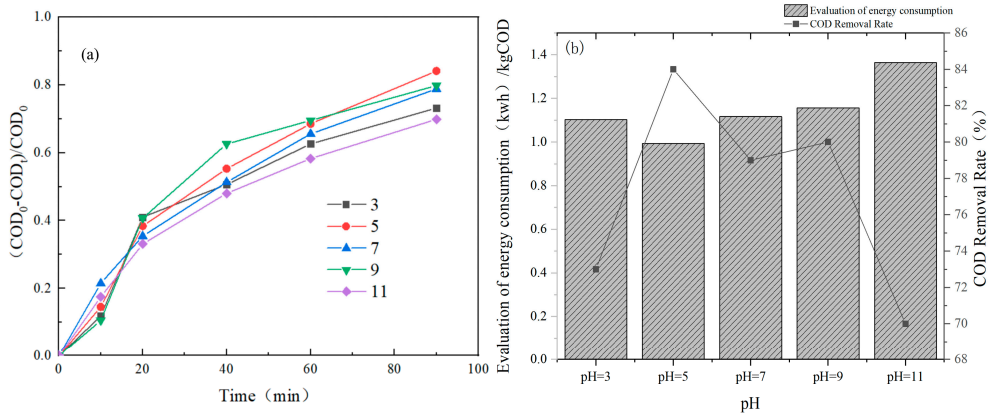

Figure 8. Effect of initial pH value on electrocatalytic oxidation performance: (**a**) COD removal efficiency and (**b**) energy consumption.

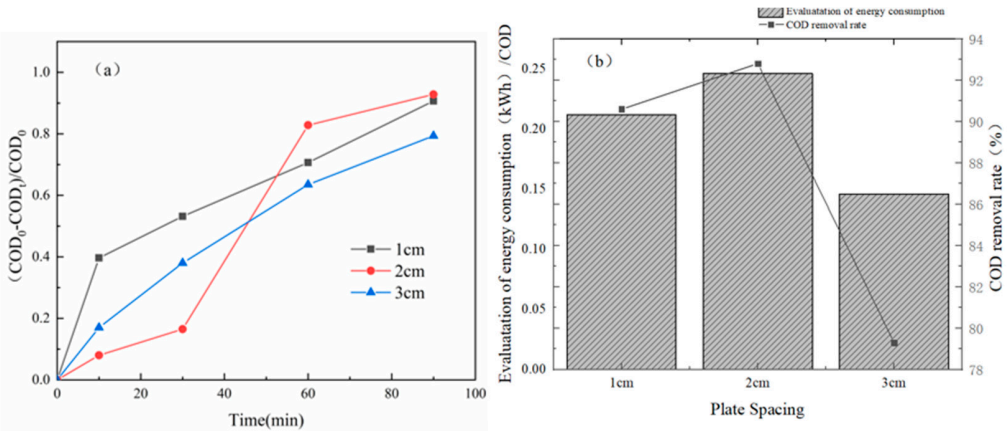

Figure 9. Effect of plate spacing on electrocatalytic oxidation performance: (**a**) COD removal efficiency and (**b**) energy consumption.

As observed from Figure 9b, the energy consumption of this system was 0.149 (kW h)/kgCOD with the plate spacing of 3 cm. When the plate spacing decreased to 2 cm, the energy consumption was decreased to 0.146 (kW h)/kgCOD. However, the further decrease in plate spacing to 1 cm significantly increased the energy consumption to 0.246 (kW h)/kgCOD. Based on the above analysis, the optimal electrode spacing for electrocatalytic oxidation reactions was 2 cm [28].

3.7. Response Surface Methodology Design and Experimental Results

3.7.1. Interaction Effects of Operating Parameters on COD Removal Efficiency

The pairwise interactions among current density (A), initial pH (B), and salt concentration (C) were analyzed using Design-Expert 13. In the response surface methodology (RSM), one factor was maintained at its center level, while the other two were varied within the experimental range. Three-dimensional response surfaces and corresponding contour plots were used to evaluate the interaction effects of the variables and identify the optimal operating region. In general, a steeper response surface indicates a greater influence of the factor on the response, whereas elliptical contour lines suggest a significant interaction between two variables.

(1) Interaction between current density and pH

Figure 10 shows the combined effects of current density and pH on COD removal efficiency. The curved response surface and elliptical contour lines indicate a significant interaction between these two factors. Within the investigation range, COD removal efficiency increased with increasing current density and decreasing pH.

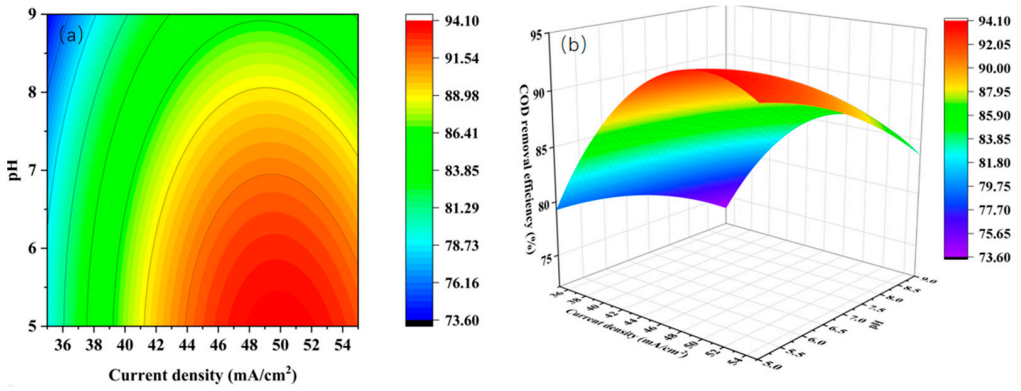

Figure 10. Response surface analysis of the effects of current density and pH on COD removal efficiency: (**a**) contour plot and (**b**) 3D surface plot.

As shown in Tables 2 and 3,the response surface varied more sharply along the pH axis than along the current density axis, indicating that pH had a stronger effect on COD removal efficiency, which is consistent with the ANOVA results. Increasing the current density from 36 to 54 mA/cm^2 enhanced the generation of reactive oxidizing species, such as ·OH and active chlorine, thereby promoting the degradation of organic pollutants. In contrast, lower pH favored higher COD removal because acidic conditions increase the oxidation potential of ·OH and suppress the competing oxygen evolution reaction. Under alkaline conditions, the activity of reactive species is weakened, resulting in lower removal efficiency.

(2) Interaction between current density and salt concentration

Figure 11 presents the effect of the interaction between current density and salt concentration on COD removal efficiency. The elongated contour lines along the salt concentration axis indicate that the interaction between these two factors was relatively weak. The response surface was much steeper along the current density axis, confirming that current density had a greater effect on COD removal efficiency than salt concentration.

The optimal region was observed at a current density of 48–54 mA/cm^2 and a pH of 5.0–6.0,where the COD removal efficiency exceeded 91.54%.

Table 2. Variance analysis of the second-order response surface regression model.

Source of Variance	Quadratic Sum	Free Degree	Mean Square	F-Number	*p*-Number	
model	665.64	9	73.96	51.73	<0.0001	significant
A	234.47	1	234.47	163.98	<0.0001	
B	91.01	1	91.01	63.65	<0.0001	
C	22.04	1	22.04	15.41	0.0057	
AB	3.08	1	3.08	2.16	0.1855	
AC	2.89	1	2.89	2.02	0.1981	
BC	1.83	1	1.83	1.28	0.2947	
A^2	149.09	1	149.09	104.27	<0.0001	
B^2	6.65	1	6.65	4.65	0.0680	
C^2	3.96	1	3.96	2.77	0.1400	
residual	10.01	7	1.43			
Mismatches term	10.23	4	3.27	3.11	0.1725	not significant
deviation	2.88	2	1.44			
Total Deviation	675.64	16				

Table 3. Analysis of variance for the response surface model.

Response Value Indicator	SD	R^2	$R_{adj}{}^2$	$R_{pre}{}^2$	C.V.%	Adeq Precision
Overall Score	1.20	0.9852	0.9661	0.8612	1.38	22.4640

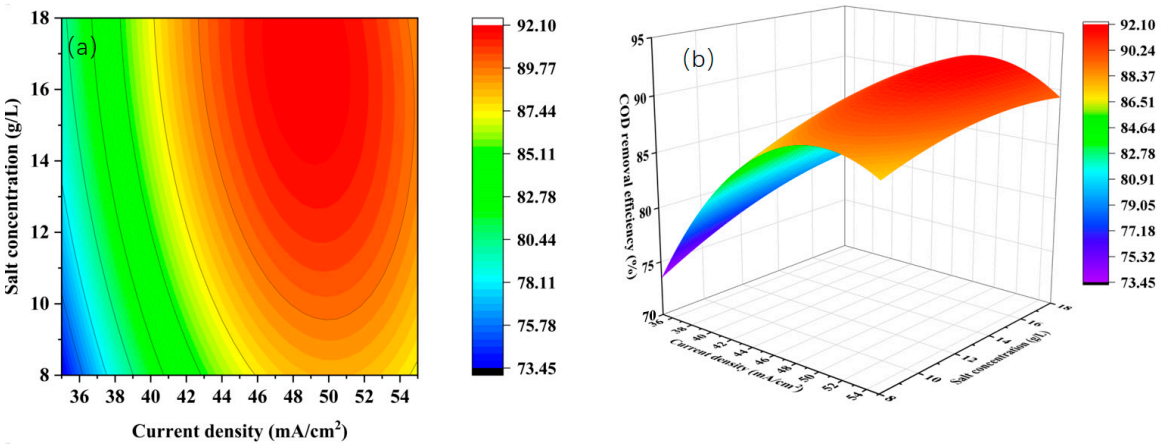

Figure 11. Response surface analysis of the effects of current density and salt concentration on corrosion resistance: (**a**) contour plot and (**b**) 3D surface plot.

As the current density increased from 36 to 54 mA/cm^2, the COD removal efficiency increased significantly due to the enhanced formation of oxidative species at the electrode surface. By contrast, increasing the salt concentration from 8 to 18 g/L resulted in only a slight improvement in COD removal. This can be attributed to the increased conductivity of the electrolyte and the facilitated formation of active chlorine species. However, within this concentration range, the conductivity was already sufficient for effective electrocatalytic oxidation, and salt concentration was no longer the rate-limiting factor. Moreover, excessive salt concentration may promote competing side reactions, such as chlorine evolution, thereby reducing its marginal benefit.

The highest COD removal efficiency (89.77–92.10%) was obtained at relatively high current density (>48 mA/cm^2) and medium-to-high salt concentration.

(3) Interaction between pH and salt concentration

Figure 12 illustrates the interaction between pH and salt concentration on COD removal efficiency. The nearly linear and uniformly distributed contour lines indicate that

the interaction between these two factors was weak. The response surface changed much more noticeably along the pH axis than along the salt concentration axis, suggesting that pH was the dominant factor affecting COD removal efficiency.

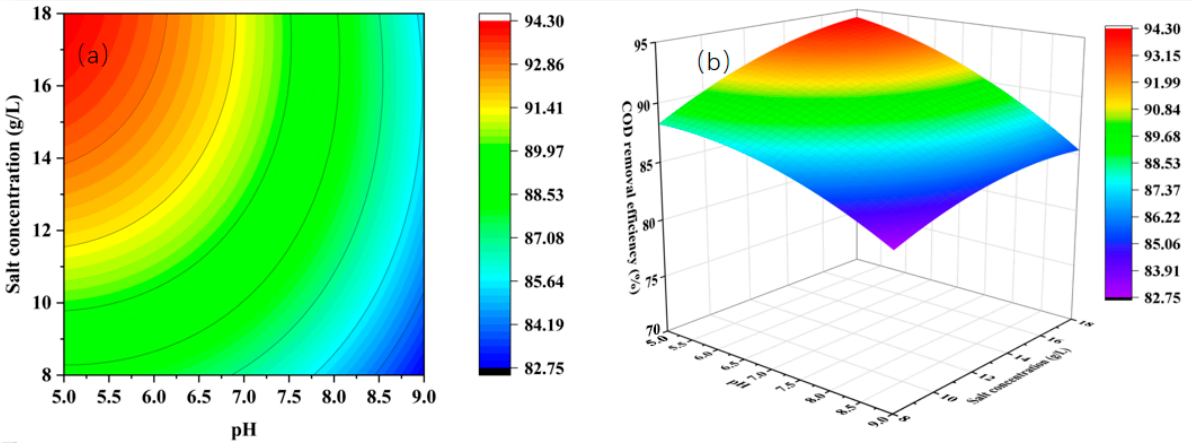

Figure 12. Response surface analysis of the effects of pH and salt concentration on COD removal efficiency: (**a**) contour plot and (**b**) 3D surface plot.

COD removal efficiency increased significantly with decreasing pH, which was mainly because acidic conditions enhance the oxidation capacity of reactive species and suppress the oxygen evolution side reaction. In contrast, increasing the salt concentration within the range of 8–18 g/L produced only a slight increase in COD removal efficiency, indicating that its effect on electrolyte conductivity and active chlorine generation was limited under the tested conditions.

The best performance was achieved at low pH and relatively high salt concentration. As shown in Figure 12, the highest COD removal efficiency (92.86–94.30%) was obtained at a pH of approximately 5.0 and a salt concentration of 16–18 g/L. Therefore, pH should be prioritized over salt concentration during process optimization.

3.7.2. Interaction Effects of Operating Parameters on Average Energy Consumption

(1) Interaction between current density and pH

Figure 13 illustrates the combined effects of current density and pH on average energy consumption (kWh/kg COD). The inclined and non-uniform contour lines indicate a strong interaction between these two factors, which is consistent with the highly significant AB interaction term identified by ANOVA. Within the investigation range, the average energy consumption increased markedly with increasing current density, whereas the effect of pH varied depending on the current density level.

As shown in Tables 4 and 5,The response surface changed much more steeply along the current density axis than along the pH axis, indicating that current density was the dominant factor affecting energy consumption. As the current density increased from 36 to 54 mA/cm^2, the average energy consumption rose sharply. This is mainly attributed to the increased current passing through the electrode area, which intensifies ohmic loss and aggravates parasitic side reactions such as oxygen evolution, thereby increasing the non-productive energy input per unit COD removed.

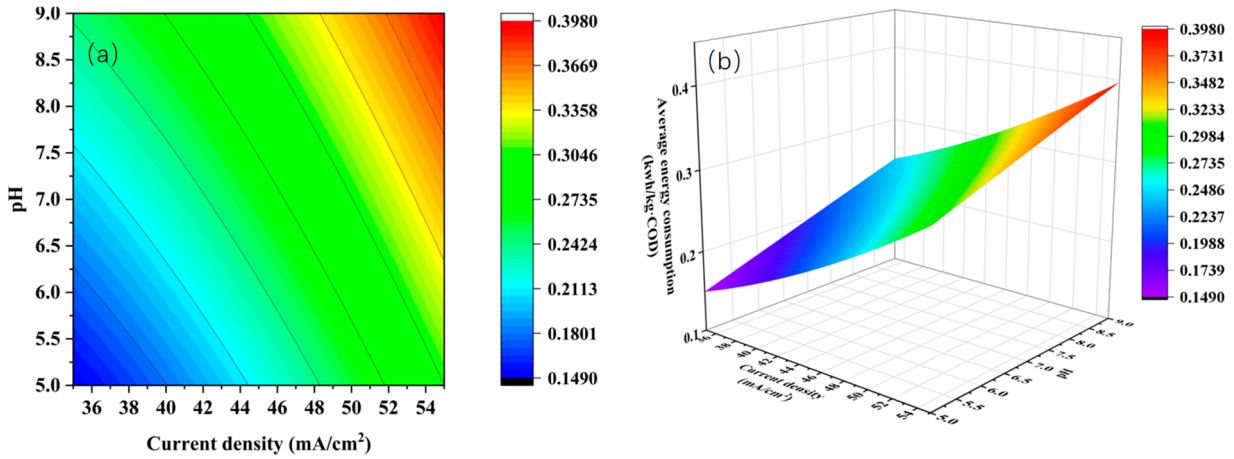

Figure 13. Response surface analysis of the effects of current density (mA/cm^2) and pH on average current efficiency: (**a**) contour plot and (**b**) 3D surface plot.

Table 4. Analysis of variance for the quadratic regression model.

Source of Variance	Quadratic Sum	Free Degree	Mean Square	F-Number	*p*-Number	
model	0.0715	9	0.0079	6678.33	<0.0001	significant
A	0.0418	1	0.0418	35,124.57	<0.0001	
B	0.0156	1	0.0156	13,124.74	<0.0001	
C	0.0011	1	0.0011	890.67	<0.0001	
AB	2.129×10^{-6}	1	2.129×10^{-6}	1.79	0.2229	
AC	3.222×10^{-6}	1	3.222×10^{-6}	2.71	0.1439	
BC	3.071×10^{-7}	1	3.071×10^{-7}	0.2581	0.6271	
A^2	0.0005	1	0.0005	383.90	<0.0001	
B^2	2.659×10^{-7}	1	2.659×10^{-7}	0.2234	0.6508	
C^2	5.470×10^{-12}	1	5.470×10^{-12}	4.596×10^{-6}	0.9983	
residual	8.331×10^{-6}	7	1.190×10^{-6}			
Mismatches term	0.48	4	3.27	7.28	0.2323	not significant
deviation	0.3216	3	0.5312			
Total Deviation	0.0715	16				

Table 5. Response surface model variance analysis table.

Response Value Indicator	SD	R^2	$R_{adj}{}^2$	$R_{pre}{}^2$	C.V.%	Adeq Precision
Overall Score	0.0011	0.9999	0.9997	0.9989	0.4023	296.2311

By comparison, pH showed a weaker influence on energy consumption. Although energy consumption slightly increased with increasing pH, its effect was much less pronounced than that of current density. The role of pH is mainly associated with changes in electrolyte properties and reaction pathways rather than direct control of any power input. Overall, lower current density and lower pH were favorable for reducing energy consumption with the minimum region located at approximately 0.15–0.18 kWh/kg COD.

(2) Interaction between current density and salt concentration

Figure 14 shows the interaction between current density and salt concentration on average energy consumption. The nearly parallel and vertically distributed contour lines indicate a weak interaction between these two factors. The average energy consumption was strongly positively correlated with current density and slightly negatively correlated with salt concentration.

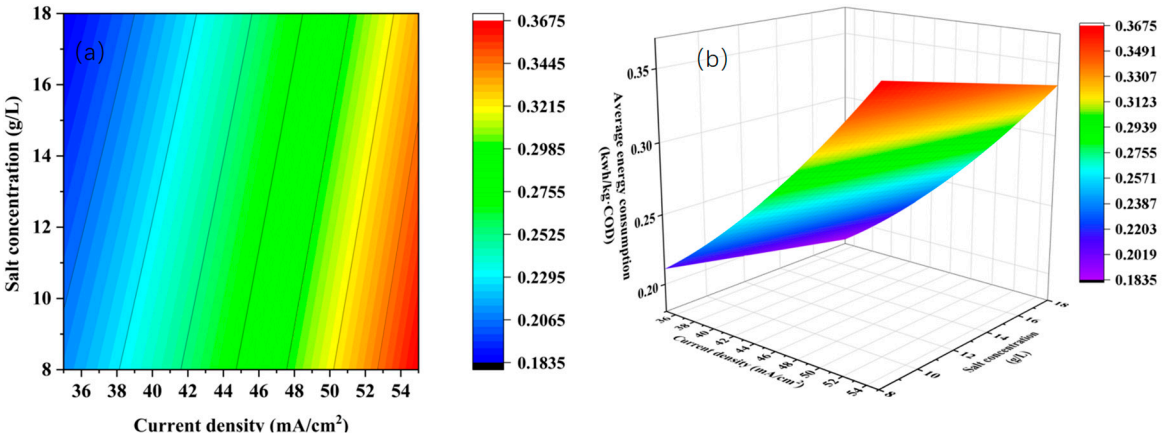

Figure 14. Response surface analysis of the effects of current density and salt concentration on average current efficiency: (**a**) contour plot and (**b**) 3D surface plot.

The response surface was much steeper along the current density axis than along the salt concentration axis, confirming that current density was the primary factor governing energy consumption. As the current density increased from 36 to 54 mA/cm^2, the energy consumption rose substantially due to increased overpotential, intensified ohmic heating, and enhanced side reactions such as oxygen evolution.

In contrast, increasing the salt concentration from 8 to 18 g/L led to a slight decrease in energy consumption. This can be attributed to the improved conductivity of the electrolyte, which reduced the cell voltage and internal resistance. According to the energy consumption relationship W = UIt, a lower cell voltage under constant current operation contributes directly to reduced energy demand. Therefore, lower current density combined with higher salt concentration was beneficial for minimizing energy consumption. The lowest energy consumption region was approximately 0.18–0.21 kWh/kg COD.

(3) Interaction between pH and salt concentration

Figure 15 presents the combined effects of pH and salt concentration on average energy consumption. The contour lines were approximately straight, uniformly spaced, and slightly inclined, indicating a weak interaction between these two variables. Energy consumption was jointly affected by pH and salt concentration, but their interaction was not significant within the studied range.

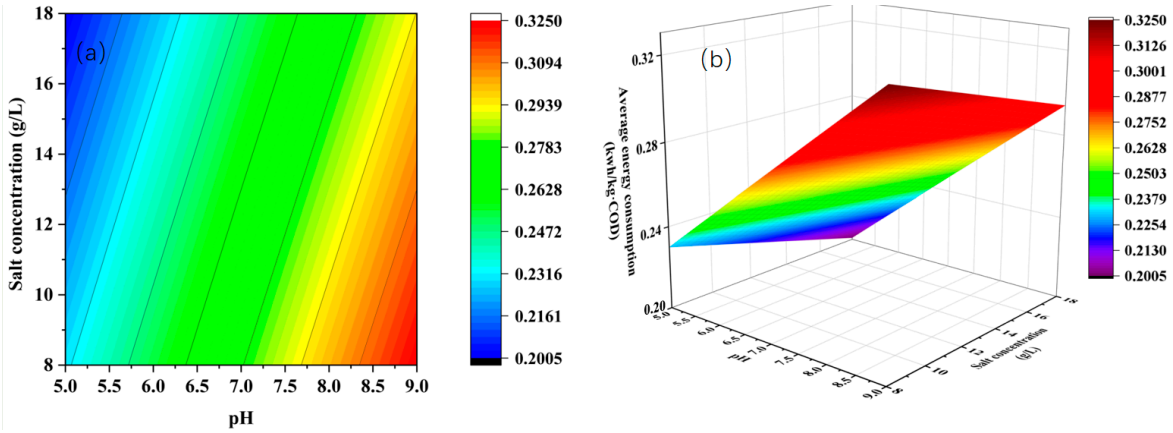

Figure 15. Response surface analysis of the effects of pH and salt concentration on average current efficiency: (**a**) contour plot and (**b**) 3D surface plot.

As the salt concentration increased from 8 to 18 g/L, the average energy consumption decreased noticeably. This is mainly because higher salt concentration improved the conductivity of the electrolyte and lowered the cell voltage, thereby reducing electrical energy consumption under galvanostatic operation. In contrast, energy consumption increased with increasing pH from 5.0 to 9.0. Lower pH likely provided a more favorable electrochemical environment for efficient energy utilization.

Overall, low pH and high salt concentration were favorable for low-energy operation. The minimum energy consumption was observed in the range of 0.2–0.21 kWh/kg COD. These results indicate that an optimal matching of current density, pH, and salt concentration is essential for achieving efficient and energy-saving wastewater treatment.

3.7.3. Process Optimization

To identify the optimal operating conditions, a multi-objective optimization method was applied. Based on the experimental results, regression models were developed to correlate current density (A), pH (B), and salt concentration (C) with COD removal efficiency (Y_1) and average energy consumption (Y_2). The optimization was performed with the objective of maximizing Y_1 while minimizing Y_2, and the optimal combination of the three factors was obtained. The objective functions and constraints are expressed as follows:

$$\begin{gathered} MaxY_1 = f(A, B, C) \\ MinY_2 = f(A, B, C) \\ s.t. \begin{cases} 35 \leq A \leq 55 \\ 5 \leq B \leq 9 \\ 8 \leq C \leq 18 \end{cases} \end{gathered}$$

Using the optimization module embedded in Design-Expert software, the optimal values of the multiple factors were determined as follows: current density (A), 43.69 mA/cm^2; pH (B), 5.0; and salt concentration (C), 15 g/L. Under these optimal conditions, the predicted COD removal efficiency and average energy consumption were 93.45% and 0.191 kWh/kg COD, respectively.

4. Mechanism Investigation

4.1. Analysis of ·OH Role in Electrochemical Catalytic Reaction

To investigate the role of hydroxyl radicals (·OH) in electrochemical oxidation processes, a common method involved adding quenchers to the system. These quenchers rapidly neutralized ·OH generation, thereby preventing its reaction with pollutants [29]. Tertiary butyl alcohol (TBA) demonstrated exceptional quenching efficacy against ·OH, serving as a highly effective quencher. By examining the impact of TBA addition on HEDP removal, it can analyze the role of ·OH oxidation in this electrochemical oxidation system [30,31]. Under the optimal experimental conditions, Figure 16 compared the effects of TBA addition versus no addition on membrane concentrate electrochemical oxidation. The results showed that after 90 min of electrochemical oxidation with TBA, the removal rate reached 59.36%, while the rate without TBA was 87.62%, indicating that the removal rate caused by ·OH oxidation was 30.26%.

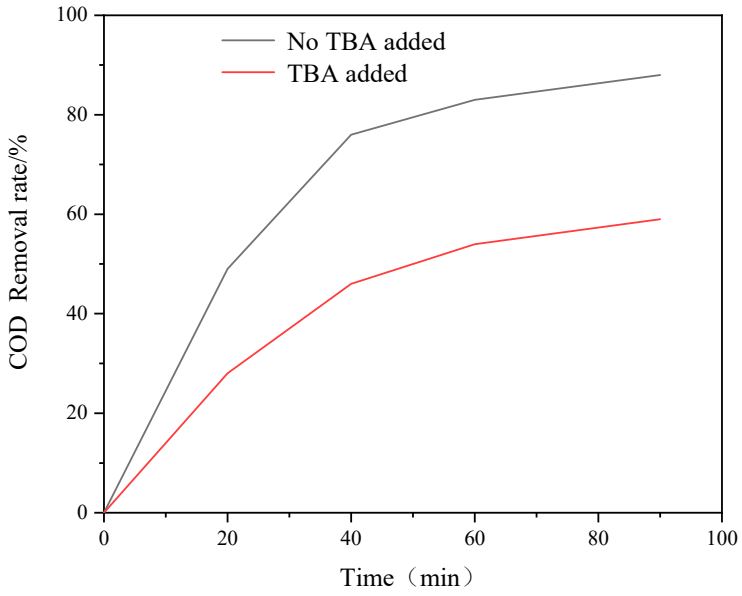

Figure 16. Effect of TBA addition on concentrate removal efficiency (current density: 45 mA/cm^2; pH: 5; electrochemical reaction time: 90 min).

4.2. Contribution of Direct Oxidation in Electrochemical Catalytic

To further investigate the mechanism of electrode electrochemical oxidation, sodium sulfate was selected as the electrolyte to simulate the quenching of active chlorine in the system, replacing sodium chloride. The charge of the electrolyte was maintained equal before and after the reaction. Since methanol (MeOH) can quench both OH^- and SO_4^{2-}, 1 mol/L MeOH with a value of quench ·OH and potential ·SO_4^{2-} was used. At this stage, the degradation kinetics of pollutants were solely driven by direct electrode oxidation [32]. The electrochemical catalytic oxidation of the membrane concentrate was conducted, and the corresponding results are shown in Figure 17. As illustrated in the figure, the removal rate of membrane concentrate after 90 min of electrochemical oxidation with MeOH addition reached 22.88%, indicating that the direct oxidation efficiency remained stable at approximately 20% during the electrochemical process, playing a secondary role rather than being dominant [33].

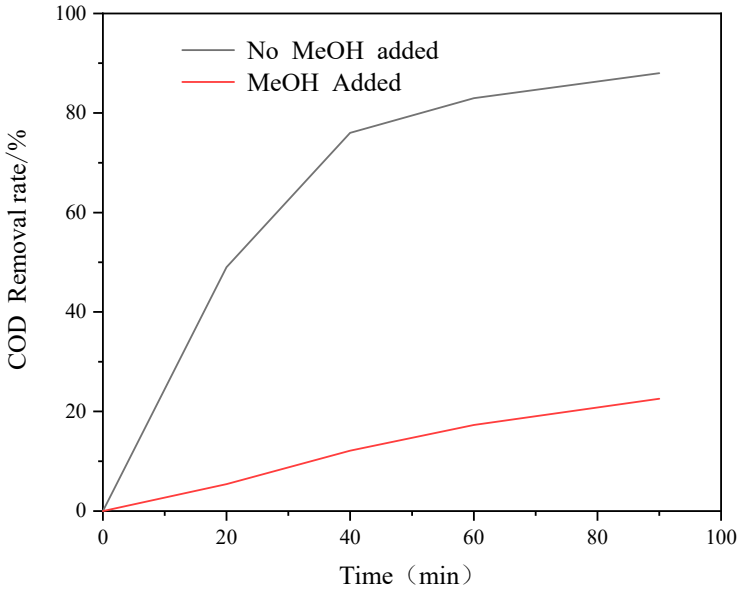

Figure 17. Effect of MeOH addition on membrane concentrate removal efficiency.

4.3. Active Chlorine Generation in Electrochemical Catalytic Processes

The reverse osmosis concentrate simulation wastewater contained sodium chloride as an electrolyte, resulting in abundant chloride ions in the reaction system. These ions generated or converted to active chlorine at the anode surface. Active chlorine, with its strong oxidizing properties, could effectively degrade organic pollutants. The previous work indicated that in chloride-containing solutions, iridium–ruthenium electrodes with low chloride evolution potential outperformed tin–antimony electrodes with high oxygen evolution potential [34]. Therefore, this experiment investigates active chlorine generation during electrochemical oxidation using Ti/IrO_2–RuO_2 electrodes. Herein, active chlorine concentration was measured via DPD spectrophotometry, and the results are presented in Figure 18. The data indicated that after 90 min of electrocatalytic reaction, the active chlorine concentration reached 1877.23 mg/L. In this system, the following electrochemical reactions occurred at the anode according to Equations (3)–(5):

$$2Cl^- \rightarrow Cl_2 + 2e^-, \quad (3)$$

$$Cl_2 + H_2O \rightarrow HOCl + Cl^- + H^+, \quad (4)$$

$$HOCl \Leftrightarrow H^+ + ClO^-, \quad (5)$$

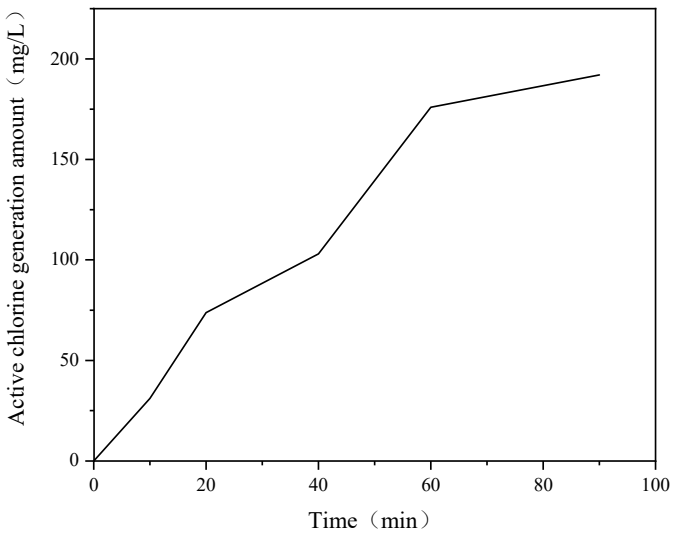

Figure 18. Variation in active chlorine generation during electrocatalytic oxidation.

The low chloride evolution potential of Ti/IrO_2–RuO_2 electrodes facilitated the reaction (4), thereby promoting active chlorine generation. However, as the reaction progresses, the rate of active chlorine production gradually decreased. Concurrently, the rising water temperature leads to the decomposition and escape rate of active chlorine exceeding its formation rate, resulting in a deceleration of the increase in active chlorine yield [35].

Thus, it was concluded that the electrode exhibited both direct and indirect oxidation mechanisms during the electrocatalytic oxidation of membrane concentrate in sodium chloride electrolyte solution. The oxidation contribution ratios of these mechanisms were calculated based on the pollutant removal rates under different time conditions. Indirect oxidation played a dominant role in the electrocatalytic degradation of membrane concentrate.

4.4. Mechanistic Analysis

Based on the above investigation, the mechanism of the electrocatalytic oxidation system is summarized as follows. As illustrated in Figure 19, during the chlorine evolution process, Ru^{4+} acted as an electron acceptor. The release of electrons from Cl^- gener-

ated Cl· and Ru^{3+}, which can subsequently be oxidized back to Ru^{4+} through the circuit. Meanwhile, Cl· participated in subsequent reactions, accelerating the chlorine evolution process [36]. Additionally, Cl^- may formed xMO (Cl·) on the electrode surface via the Volmer–Heyrovsky mechanism. However, this bound Cl· was prone to be oxidated into Cl_2.

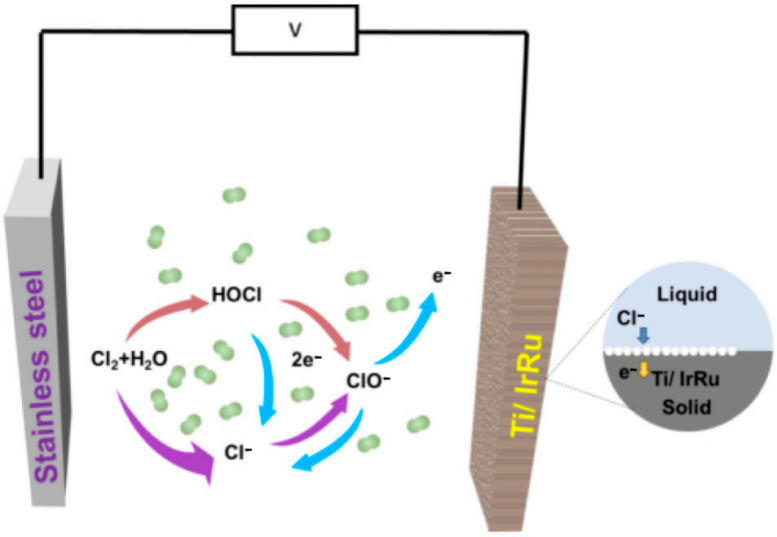

Figure 19. Mechanism diagram of electrocatalytic reaction process.

In the liquid phase, Cl_2 readily hydrolyzed to form $HClO/ClO^-$ (Equation (6) to Equation (8)) with the anode-generated HClO further reduced to Cl^-. As the pH in this experiment continuously decreased from its initial value to approximately 4, and ClO^- concentrations were low in solutions below a pH of 5, HClO became the primary product of Cl_2 hydrolysis. The Cl·species directly generated through Ru^{4+}/Ru^{3+} redox reactions, which could further react with HClO to form ClO^- [37]. Additionally, the anodic oxidation process inevitably involved water electrolysis, producing ·OH radicals on the electrode surface. These ·OH radicals subsequently reacted with HClO to generate ClO·.

$$HOCl + 2e^- \rightarrow Cl^- + OH^-, \quad (6)$$

$$Cl\bullet + HClO \rightarrow ClO\bullet + H^+ + Cl^- \quad (7)$$

$$\bullet OH + HClO \rightarrow ClO\bullet + H_2O \quad (8)$$

It was indicated that indirect oxidation played a dominant role in the electrocatalytic oxidation of membrane concentrate with active chlorine oxidation contributing more than hydroxyl radical oxidation within this indirect oxidation mechanism.

5. Conclusions

A $Ti/IrO_2–RuO_2$ anode-based electrocatalytic oxidation system was developed for the pretreatment of high-salinity pesticide and chemical membrane concentrate. The results showed that the current density, pH, salt concentration, and electrode spacing all affected system performance, among which current density and pH were the most important factors for COD removal, while current density was the dominant factor influencing energy consumption. Under the optimal conditions determined by single-factor experiments, namely a current density of 45 mA/cm^2, salt concentration of 13 g/L, initial pH of 5.0, and electrode spacing of 2 cm, the COD removal efficiency reached 92.37%. Further multi-objective optimization predicted that a current density of 43.69 mA/cm^2, pH of 5.0, and salt concentration of 15 g/L could achieve a COD removal efficiency of 93.45% with

an average energy consumption of 0.191 kWh/kg COD. Mechanistic analysis indicated that both direct and indirect oxidation participated in pollutant degradation with indirect oxidation dominating the process and active chlorine species contributing more significantly than hydroxyl radicals. Overall, the Ti/IrO_2–RuO_2 electrocatalytic system demonstrated high efficiency and low energy consumption, providing a promising approach for the pretreatment of refractory membrane concentrate from pesticide and chemical industries.

Author Contributions: Y.P.: investigation, data curation, writing—original draft. Y.C.: manuscript revision. M.Z.: writing—review and editing, resources, validation. H.Z.: validation, supervision. Z.L.: resources, methodology. Z.H.: resources, methodology. J.J.: formal analysis. All authors have read and agreed to the published version of the manuscript.

Funding: This research was funded by the National Natural Science Foundation of China (NO: U23A20605), Industry University Research Cooperation Project (NO: 2024-YJGFGC-F1066).

Data Availability Statement: The data that support the findings of this study are available from the corresponding author upon reasonable request.

Conflicts of Interest: The authors declare that there are no conflicts of interest.

References

1. Sun, Y.; Zhu, S. Degradation of high-chemical oxygen demand concentration pesticide wastewater by 3D electrocatalytic oxidation. *J. Environ. Chem. Eng.* **2019**, *7*, 103276. [CrossRef]
2. Nakano, Y.; Miyazaki, A.; Yoshida, T.; Ono, K.; Inoue, T. A study on pesticide runoff from paddy fields to a river in rural region—1: Field survey of pesticide runoff in the Kozakura River, Japan. *Water Res.* **2004**, *38*, 3017–3022. [CrossRef] [PubMed]
3. Zou, X.F.; Ma, F.; Li, Q.C.; Ji, H.D.; Zhuang, H.D.; Tan, X.; Wang, J.G.; Liu, B. Pilot-scale study of biological synergist effect onhigh salinity pesticide wastewater biological treatment. *IOP Conf. Ser. Earth Environ. Sci.* **2018**, *186*, 012005. [CrossRef]
4. Goudarzi, M.; Ghorbani, M. A study on ternary mixed oxide coatings containing Ti, Ru, Ir by sol-gel method on titanium. *J. Sol-Gel Sci. Technol.* **2015**, *73*, 332–340. [CrossRef]
5. Keyikoglu, R.; Karatas, O.; Rezania, H.; Kobya, M.; Vatanpour, V. A review on treatment of membrane concentrates generated from landfill leachate treatment processes. *Sep. Purif. Technol.* **2021**, *259*, 118182. [CrossRef]
6. Lukic, N.; Diezel, L.L.; Fröba, A.P.; Leipertz, A. Economical aspects of the improvement of a mechanical vapour compression desalination plant by dropwise condensation. *Desalination* **2010**, *264*, 173–178. [CrossRef]
7. Ahmed, Z.; Yusoff, M.S.; Kamal, N.H.M.; Aziz, H.A. Optimization of the humic acid separation and coagulation with natural starch by RSM for the removal of COD and colour from stabilized leachate. *Waste Manag. Res.* **2021**, *39*, 1396–1405. [CrossRef]
8. Dong, N.; Ye, Q.; Chen, M.; Cheng, S.; Kang, T.; Dai, H. Sodium-treated sepiolite-supported transition metal (Cu, Fe, Ni, Mn, or Co) catalysts for HCHO oxidation. *Chin. J. Catal.* **2020**, *41*, 1734–1744. [CrossRef]
9. He, C.; Cheng, J.; Zhang, X.; Douthwaite, M.; Pattisson, S.; Hao, Z. Recent advances in the catalytic oxidation of volatile organic compounds: A review based on pollutant sorts and sources. *Chem. Rev.* **2019**, *119*, 4471–4568. [CrossRef]
10. Chen, B.; Wang, S.; Liu, J.; Huang, H.; Dong, C.; He, Y.; Yang, H. Corrosion resistance mechanism of a novel porous Ti/Sn-Sb-RuO_x/β-PbO_2 anode for zinc electrowinning. *Corros. Sci.* **2018**, *144*, 136–144. [CrossRef]
11. Krastanov, A.; Alexieva, Z.; Yemendzhiev, H. Microbial degradation of phenol and phenolic derivatives. *Eng. Life Sci.* **2013**, *13*, 76–87. [CrossRef]
12. Li, Y.; Dong, H.; Li, L.; Tang, L.; Tian, R.; Li, R.; Zeng, G. Efficient degradation of sulfamethazine via activation of percarbonate by chalcopyrite. *Water Res.* **2021**, *192*, 116850. [CrossRef]
13. Ansari, A.; Nematollahi, D. Convergent paired electrocatalytic degradation of p-dinitrobenzene by Ti/SnO_2-Sb/β-PbO_2 anode. A new insight into the electrochemical degradation mechanism. *Appl. Catal. B Environ.* **2020**, *261*, 118226. [CrossRef]
14. Jun, M.; Nigel, J.D.G. Degradation of atrazine by manganese-catalysed ozonation influence of radical scavengers. *Water Res.* **2000**, *34*, 3822–3828. [CrossRef]
15. Chen, Z.W.; Li, J.; Ou, P.; Huang, J.E.; Wen, Z.; Chen, L.; Jiang, Q. Unusual Sabatier principle on high entropy alloy catalysts for hydrogen evolution reactions. *Nat. Commun.* **2024**, *15*, 359. [CrossRef] [PubMed]
16. Sun, W.; Ma, B.; Sun, Y.; Zheng, H.; Ma, G. Electrochemical degradation of tetracycline by gamma-Al_2O_3-Bi-(Sn/Sb) three-dimensional particle electrode. *Desalin. Water Treat.* **2017**, *98*, 152–160. [CrossRef]
17. Liu, H.; Li, X.; Peng, C.; Zhu, L.; Zhang, Y.; Cheng, H.; Lu, Y. Activating the lattice oxygen in $(Bi_{0.5}Co_{0.5})_2O_3$ by vacancy modulation for efficient electrochemical water oxidation. *J. Mater. Chem. A* **2020**, *8*, 13150–13159. [CrossRef]

18. Liu, D.; Zhou, S. Visible light-driven photoelectrocatalysis coupling with electroenzymatic process for degradation of chloramphenicol. *Chem. Eng. J.* **2017**, *330*, 1380–1389. [CrossRef]
19. Li, J. Oxygen Evolution reaction in energy conversion and storage: Design strategies under and beyond the energy scaling relationship. *Nano-Micro Lett.* **2022**, *14*, 112. [CrossRef]
20. Zhao, Z.; Zhou, H.; Zheng, L.; Niu, P.; Yang, G.; Hu, W.; Ran, J.; Qiao, S.; Wang, J.; Zheng, H. Molecules interface engineering derived external electric field for effective charge separation in photoelectrocatalysis. *Nano Energy* **2017**, *42*, 90–97. [CrossRef]
21. Grimaud, A.; Diaz-Morales, O.; Han, B.; Hong, W.T.; Lee, Y.-L.; Giordano, L.; Stoerzinger, K.A.; Koper, M.T.M. Activating lattice oxygen redox reactions in metal oxides to catalyse oxygen evolution. *Nat. Chem.* **2017**, *9*, 457–465. [CrossRef]
22. León, I.; Gomes, H.; Sepúlveda-Guzmán, S. Electro-oxidation of amoxicillin using titanium electrodes electrophoretically coated by iridium or ruthenium with tantalum oxides. *J. Chem. Technol. Biotechnol.* **2020**, *34*, 622–629. [CrossRef]
23. Chou, K.W.; Norli, I.; Anees, A. Evaluation of the effect of temperature, NaOH concentration and time on solubilization of palm oil mill effluent (POME) using response surface methodology (RSM). *Biotechnol. Bioeng.* **2010**, *101*, 8616–8622. [CrossRef] [PubMed]
24. Tan, X.; Zhang, M.; Chen, D.; Li, W.; Gou, W.; Qu, Y.; Ma, Y. Electrochemical etching switches electrocatalytic oxygen evolution pathway of $IrOx/Y_2O_3$ from adsorbate evolution mechanism to Lattice-Oxygen-Mediated Mechanism. *Small* **2023**, *19*, 2303249. [CrossRef]
25. Ventura, A.; Jacquet, G.; Bermond, A.; Camel, V. Electrochemical generation of the Fenton's reagent: Application to atrazine degradation. *Water Res.* **2002**, *36*, 3517–3522. [CrossRef] [PubMed]
26. Chen, G.H. Electrochemical technologies in wastewater treatment. *Sep. Purif. Technol.* **2004**, *38*, 11–14. [CrossRef]
27. Tang, X.; Wu, Q.Y.; Du, Y.; Yang, Y.; Hu, H.Y. Anti-estrogenic activity formation potential assessment and precursor analysis in reclaimed water during chlorination. *Water Res.* **2014**, *48*, 490–497. [CrossRef] [PubMed]
28. Chen, W.; Westerhoff, P.; Leenheer, J.A.; Booksh, K. Fluorescence excitation-emission Matrix regional integration to quantify spectra for Dissolved Organic Matter. *Environ. Sci. Technol.* **2003**, *37*, 5701–5710. [CrossRef]
29. Wu, Y.; Yao, R.; Zhao, Q.; Li, J.; Liu, G. RuO_2 nanoparticles anchored on g-C_3N_4 as an efficient bifunctional electrocatalyst for Water Splitting in acidic media. *Dalton Trans.* **2023**, *52*, 10515–10521. [CrossRef] [PubMed]
30. Zhang, M.; Chen, J.; Li, H.; Cai, P.; Li, Y.; Wen, Z. Ru-RuO_2/CNT hybrids as high-activity pH-universal electrocatalysts for water splitting within 0.73 V in an asymmetric-electrolyte electrolyzer. *Nano Energy* **2019**, *61*, 576–583. [CrossRef]
31. Cheng, W.; Yang, M.; Xie, Y.; Liang, B.; Fang, Z.; Tsang, E.P. Enhancement of mineralization of metronidazole by the electro-Fenton process with a Ce/SnO_2-Sb coated titanium anode. *Chem. Eng. J.* **2013**, *220*, 214–220. [CrossRef]
32. Cai, J.; Zhou, M.; Pan, Y.; Du, X.; Lu, X. Extremely efficient electrochemical degradation of organic pollutants with co-generation of hydroxyl and sulfate radicals on Blue-TiO_2 nanotubes anode. *Appl. Catal. B Environ.* **2019**, *257*, 117902. [CrossRef]
33. Li, X.; Duan, P.; Lei, J.; Sun, Z.; Hu, X. Fabrication of Ti/TiO_2/SnO_2-Sb-Cu electrode for enhancing electrochemical degradation of ceftazidime in aqueous solution. *J. Electroanal. Chem.* **2019**, *847*, 113231. [CrossRef]
34. Chen, J.; Qi, M.; Yang, Y.; Xiao, X.; Li, Y.; Jin, H.; Wang, Y. Chloride Residues in RuO_2 Catalysts Enhance Its Stability and Efficiency for Acidic Oxygen Evolution Reaction. *Angew. Chem. Int. Ed.* **2025**, *64*, e202420860. [CrossRef] [PubMed]
35. de Moura, D.; de Araújo, C.; Zanta, C.; Martínez-Huitle, R. Active chlorine species electrogenerated on Ti/$Ru_{0.3}Ti_{0.7}O_2$ surface: Electrochemical behavior, concentration determination and their application. *J. Electroanal. Chem.* **2014**, *731*, 145–152. [CrossRef]
36. Hao, X.; Quansheng, Y.; Dan, S.; Honghui, Y.; Jidong, L.; Jiangtao, F.; Wei, Y. Fabrication and characterization of PbO_2 electrode modified with $[Fe(CN)_6]^{3-}$ and its application on electrochemical degradation of alkali lignin. *J. Hazard. Mater.* **2015**, *286*, 509–516. [CrossRef] [PubMed]
37. Xu, L.; Wang, Y.; Xu, Q.T.; Hu, H.Y. Comparison of the properties of low-dimensional nano-Ti/SnO_2-Sb-Fe electrodes prepared by different methods. *J. Electrochem. Soc.* **2019**, *166*, E69–E76. [CrossRef]

Disclaimer/Publisher's Note: The statements, opinions and data contained in all publications are solely those of the individual author(s) and contributor(s) and not of MDPI and/or the editor(s). MDPI and/or the editor(s) disclaim responsibility for any injury to people or property resulting from any ideas, methods, instructions or products referred to in the content.